

High-resolution spectroscopy of flares and CMEs on AD Leo[★]

P. Muheki^{1,2}, E.W. Guenther¹, T. Mutabazi², and E. Jurua²

¹ Thüringer Landessternwarte Tautenburg, Sternwarte 5, 07778 Tautenburg, Germany

² Mbarara University of Science and Technology, P.O Box 1410, Mbarara, Uganda

e-mail: pmuheki@must.ac.ug; guenther@tls-tautenburg.de; ejurua@must.ac.ug

Preprint online version: February 1, 2022

ABSTRACT

Context. Flares and coronal mass ejections (CMEs) are important for the evolution of the atmospheres of planets and their potential habitability, particularly for planets orbiting M stars at a distance < 0.4 AU. Detections of CMEs on these stars have been sparse, and previous studies have therefore modelled their occurrence frequency by scaling up solar relations. However, because the topology and strength of the magnetic fields on M stars is different from that of the Sun, it is not obvious that this approach works well.

Aims. We used a large number of high-resolution spectra to study flares, CMEs, and their dynamics of the active M dwarf star AD Leo. The results can then be used as reference for other M dwarfs.

Methods. We obtained more than 2000 high-resolution spectra ($R \sim 35000$) of the highly active M dwarf AD Leo, which is viewed nearly pole on. Using these data, we studied the behaviour of the spectral lines H_{α} , H_{β} , and $He I 5876$ in detail and investigated asymmetric features that might be Doppler signatures of CMEs.

Results. We detected numerous flares. The largest flare emitted 8.32×10^{31} erg in H_{β} and 2.12×10^{32} erg in H_{α} . Although the spectral lines in this and other events showed a significant blue asymmetry, the velocities associated with it are far below the escape velocity.

Conclusions. Although AD Leo shows a high level of flare activity, the number of CMEs is relatively low. It is thus not appropriate to use the same flare-to-CME relation for M dwarfs as for the Sun.

Key words. Techniques: spectroscopic – Stars: activity – Stars: flares – Stars: late-type – Stars: individual: AD Leo

1. Introduction

Observations with the Kepler and CoRoT satellites have shown that extrasolar planets are much more diverse than the planets in our Solar System (Lammer et al. 2011). This large diversity especially in density is particularly striking for planets in the mass range between 1 and $15 M_{\text{Earth}}$ (Hatzes & Rauer 2015). In this mass range, planets can have low densities, for example, Kepler-51 (0.05 g cm^{-3} , Masuda 2014), or very high densities (K2-106, $13.1_{-3.6}^{+5.4} \text{ g cm}^{-3}$, Guenther et al. 2017; K2-229b, $8.9 \pm 2.1 \text{ g cm}^{-3}$, Santerne et al. 2018; Kepler-107c, $12.65 \pm 2.45 \text{ g cm}^{-3}$, Bonomo et al. 2019). This large diversity in densities is obviously related to different compositions of the planets. The high-density planets must be rocky and cannot have a dense, extended atmosphere. In contrast to this, planets with low density must correspondingly have extended atmospheres that mostly consist of H_2/He (Lissauer et al. 2011; Lammer et al. 2011). The large variation in the structure of planets must be related to their formation and evolution. High-density planets either never had an extended H_2/He atmosphere or lost it when they were young (Lissauer et al. 2011). Perhaps both scenarios play a role.

Many studies (e.g. Lammer et al. 2008, 2014) have shown that atmospheric loss processes are important for the evolution of planets. Low-mass planets such as CoRoT-7b, which orbits within 0.02 AU, could lose their atmosphere by extreme ultra-violet (EUV) and X-ray driven photoevaporation or in a

boil-off event (e.g. Lammer et al. 2013; Kislyakova et al. 2013; Erkaev et al. 2016; Roettenbacher & Kane 2017). For example, Roettenbacher & Kane (2017) showed for the TRAPPIST-1 system that the environment has potentially led to the erosion of the atmospheres of planets in the habitable zone through EUV stellar emission. Bolmont et al. (2017) further showed that TRAPPIST-1b and c may have lost about 15 Earth oceans, but TRAPPIST-1d about less than one Earth ocean. These planets could thus only have water if the original water contents were one or a few Earth oceans higher than that. However, the simulation by Tian & Ida (2015) showed that M stars are expected to have two types of planets in the habitable zones: ocean planets without continents, and desert planets, on which there is orders of magnitude less surface water than on Earth. Most of the observational studies (e.g. France et al. 2012; Roettenbacher & Kane 2017; Bolmont et al. 2017) have concentrated on X-ray and EUV radiation (XUV radiation) of the stars in quiescence, but flares and coronal mass ejections (CMEs) certainly play a role as well (Lammer et al. 2007, 2009a).

Flares affect the potential habitability of planets in many ways, and these effects are particularly important for planets orbiting M stars. According to Tuomi et al. (2019), three planets on average orbit M stars. These stars have a relatively high activity, but the potentially habitable planets orbit at considerably small distance ($\sim 0.03 \text{ AU} - 0.4 \text{ AU}$) (e.g. Segura et al. 2010; Vida et al. 2017; Howard et al. 2018; Tuomi et al. 2019). The importance of flares on M dwarfs is underlined by the fact that they might dominate the far-UV (FUV) energy budget (Lloyd et al. 2018). An interesting example for the effect of

[★] Based on observations obtained at the Thüringer Landessternwarte Tautenburg, Germany

flares on the habitability of planets is TRAPPIST-1 (Gillon et al. 2016). Vida et al. (2017) showed for this star that the flare activity is so high that the atmospheres of the planets orbiting in the habitable zone may be continuously altered, making them less favourable for hosting life. Another interesting example is Proxima Centauri. Kielkopf et al. (2019) observed a superflare on this star in which the energy of the flare was 100 times the star's luminosity, and such large flares may endanger life on a planet in the habitable zone.

On the other hand, the erosion of planetary atmospheres caused by CMEs (due to ion-pick up) depends on the plasma densities and flow velocities of the CMEs, and the magnetic moments of the planets (Lammer et al. 2009b). As shown by Kay et al. (2016), exoplanets around M dwarfs would require magnetic fields of between tens and hundreds of Gauss to protect them against CMEs, but because close-in planets are tidally locked (Lammer et al. 2007; Barnes 2017), it is generally thought that their magnetic moments are relatively low. According to Lammer et al. (2014), planets with an Earth-like structure orbiting an M star may lose their entire atmosphere as a result of CMEs. This is based on the assumption that the CME rate is 100 times higher than that of the Sun because the X-ray brightness of such stars is 100 times higher. However, it is not certainly known what the CME rate of M dwarfs really is.

Previous studies (e.g. Aarnio et al. 2012; Drake et al. 2013; Leitzinger et al. 2014; Osten & Wolk 2015; Odert et al. 2017; Crosley & Osten 2018) used the correlations between solar flare energies and CME parameters to estimate possible occurrence frequencies of CMEs in M stars. However, it is still uncertain whether it is correct to use the solar analogy for these very active stars. Solar CMEs originate from regions that have a very specific magnetic field geometry, that is, regions of complex magnetic topology and high field strength (Aarnio et al. 2012). The topology of fully convective M dwarfs is very complex and divergent (Morin et al. 2008, 2010). Rapidly rotating M dwarfs have several kiloGauss large-scale magnetic fields at high latitudes, and their coronae are dominated by star-size large hot loops (Cohen et al. 2017). In addition to this, active M dwarfs with dipole-dominated axisymmetric field topologies can undergo a long-term global magnetic field variation (Lavail et al. 2018). Because the topology of the magnetic fields in M dwarfs may differ from that of the Sun, and because the release of matter in CMEs requires certain field geometries of the overlying magnetic field (Odert et al. 2017), it is not obvious that it is possible to use the solar analogy to estimate the effect of CMEs on planets orbiting M dwarfs. A much better approach is to study energies, velocities, and masses of CMEs during flare events on active M dwarfs and to extrapolate these results to the less active M dwarfs. Loyd et al. (2018) showed that when flare energies were normalised by the star's quiescent flux, the active and inactive samples exhibited identical slopes of the cumulative flare frequency distribution. Thus it is possible to study active M dwarfs and extrapolate the results to less active ones.

The spectroscopic signature of CMEs are blue-shifted components where the velocity shift exceeds the escape velocity of the star (Vida et al. 2019, and references there in). CMEs have been observed on M dwarfs (e.g. Houdebine et al. 1990; Cully et al. 1994; Gunn et al. 1994; Guenther & Emerson 1997; Vida et al. 2016), but all these were serendipitous events and thus are not enough for a statistical inference on their occurrence rate. Vida et al. (2016) showed that the observed CME rate is much lower than the expected rate derived from the CME-flare ratio on the Sun. Given the expected low rate of such events, we need to observe the stars for a long time, but even then it is use-

ful to observe a particularly active star in order to observe more flares and CMEs.

For this study we selected the highly active M4 dwarf AD Leo (=GJ 388) (Keenan & McNeil 1989; Lurie et al. 2014). A spectropolarimetric study by Morin et al. (2008) showed that the star is seen nearly pole-on. The field is poloidal with or without the presence of a toroidal component that accounts for 1-5% of the magnetic energy. This star's high activity and the field geometry orientation increase the chances for observing CMEs compared to other M dwarfs.

AD Leo has been the subject of a number of flare studies. On April 12, 1985, Hawley & Pettersen (1991) observed a flare that released 9.8×10^{-8} erg cm $^{-2}$ in H $_{\alpha}$ and 1245×10^{-8} erg cm $^{-2}$ in total. Hawley et al. (2003) studied flares on AD Leo using multi-wavelength simultaneous photometry and high-resolution spectroscopy. They studied 8 sizeable flares in four nights of observation, giving insights into the correlation between continuum and line emission in the optical and ultraviolet wavelengths. A detailed spectroscopic study of the flares on AD Leo was also presented by Crespo-Chacón et al. (2006). During the 16.1 hours of monitoring time, the authors obtained 600 spectra and observed 14 flares. The energies of the flares range from 1.5 to 8.2×10^{29} erg in H $_{\beta}$. The resolution of the blue spectra that include H $_{\beta}$ was $R \sim 4400$, and that of the red spectra that cover H $_{\alpha}$ was $R \sim 5600$. While these spectra allow measuring the line fluxes, the resolution is not high enough to study the subtle changes of the line profiles. Buccino et al. (2014) studied the chromospheric activity of AD Leo using medium-resolution echelle spectra taken over a period of 13 years. However, they focused on studying the variations in the activity, thereby neglecting spectra that had flares.

Extreme ultra-violet radiation causes the atmospheric loss processes by heating the upper atmospheres of the planets. However, it is difficult to observe and monitor active M stars for a long time at these wavelengths. Moreover, stellar CMEs can be detected using spectroscopy by studying Doppler shifts and line asymmetries with enhanced blue wings of the stellar emission lines. When the component is blue-shifted by more than the escape velocity, we can be certain that this material is ejected by the star. We therefore used optical observations to study the flare rates, their energies, and the CMEs, which can then be used in models to calculate the atmospheric loss rates. The Balmer lines are ideally suited for this purpose because we know from solar observations that these lines are closely related to the XUV radiation because the H $_{\alpha}$ loops are located just below the X-ray loops and thus are heated by XUV radiation from above (Butler 1993).

We present here a comprehensive study of the flare activity of AD Leo using high-resolution spectra taken over a long observing period. This enabled us to detect much smaller wavelength shifts and thus gain more insight into CME dynamics on this star.

2. Observations and data reduction

AD Leo is one of the stars that was monitored during the flare-search program of the Thüringer Landessternwarte. For this program we used the 2m Alfred Jensch telescope of the Thüringer Landessternwarte Tautenburg, which is equipped with an échelle spectrograph with a resolving power of $R \sim 35000$, and we used the 2'' slit. The spectra cover the wavelength region from 4536 to 7592 Å. With a resolution of 8.5 km s $^{-1}$, it is possible to detect CMEs and also study more subtle changes of the line profiles during such events. Spectra were obtained in various campaigns

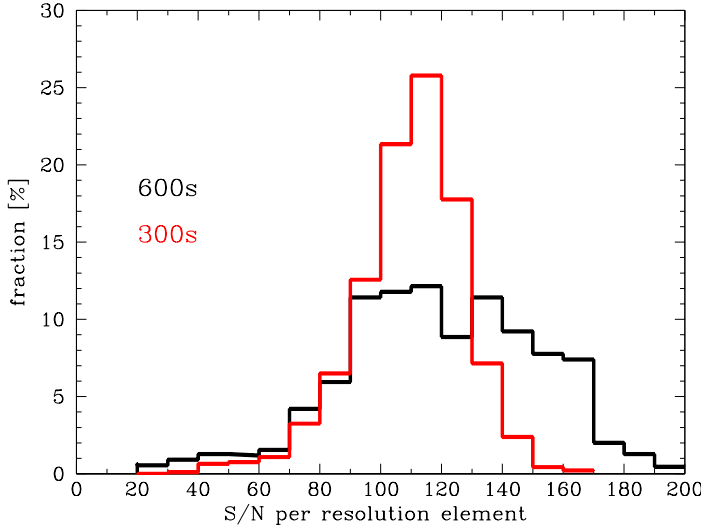


Fig. 1. Variation of the S/N per resolution element of the spectra.

from November 2016 until February 2019. Observations were typically scheduled for one week per month, when the object was visible. When possible, AD Leo was observed continuously throughout the night. The exposure times were initially set to 600 s, but after the large event observed in February 2018, we decided to reduce the exposure time to 300 s in order to obtain a better sampling of the rise times of the flares. We thus obtained 862 spectra with 600 s exposure time and a monitoring time of 143.7 h. Since April 2018, we have monitored AD Leo for 95 h, obtaining 1140 spectra with 300 s exposure time. The total monitoring time was thus 238.7 h in 57 nights of observation. A log of the observations is given in Table 1. In Fig. 1 we show the variation of the signal-to-noise ratio (S/N) per resolution element.

The spectra obtained were bias-subtracted, flat-fielded, the scatter light removed and extracted using standard IRAF routines. Spectra taken with a ThAr lamp were used for the wavelength calibration.

3. Results

3.1. Flare observations

AD Leo shows a very high level of chromospheric activity, especially in the Balmer lines (H_α and H_β) and the He I D_3 , and we therefore studied the behaviour of these three lines. In order to detect flares in AD Leo, we measured the fluxes in the H_α , H_β , and He I D_3 lines and used them to construct light curves.

Examples of the relative flux variation in H_α of the flares are shown in Fig. 2. As is typical for flares, not all the events show the classical light curve (panel 2) of a sudden increase and slow decrease, but often a more complex structure (panel 1). Figure 2 shows two nights in which multiple events occurred (e.g. panels 5-8). The enhancement in the He I 5876 emission line (see Fig. 3) shows that a plasma that is much hotter than the photosphere is present during these events. The He I 5876 emission line occurs at about 20000 K (Giampapa et al. 1978). However, we did not detect the He II 4686 line, which requires a temperature of 30000 K to be excited (Lamzin 1989). This means that the plasma was not hot enough to excite this line. In addition to the unfavourable weather conditions that interrupted the observations especially in 2016, the activity seems to be lower in 2016 and 2017 than in 2018 and 2019. There is an increase in the activity levels beginning in February 2018 (see Table 1).

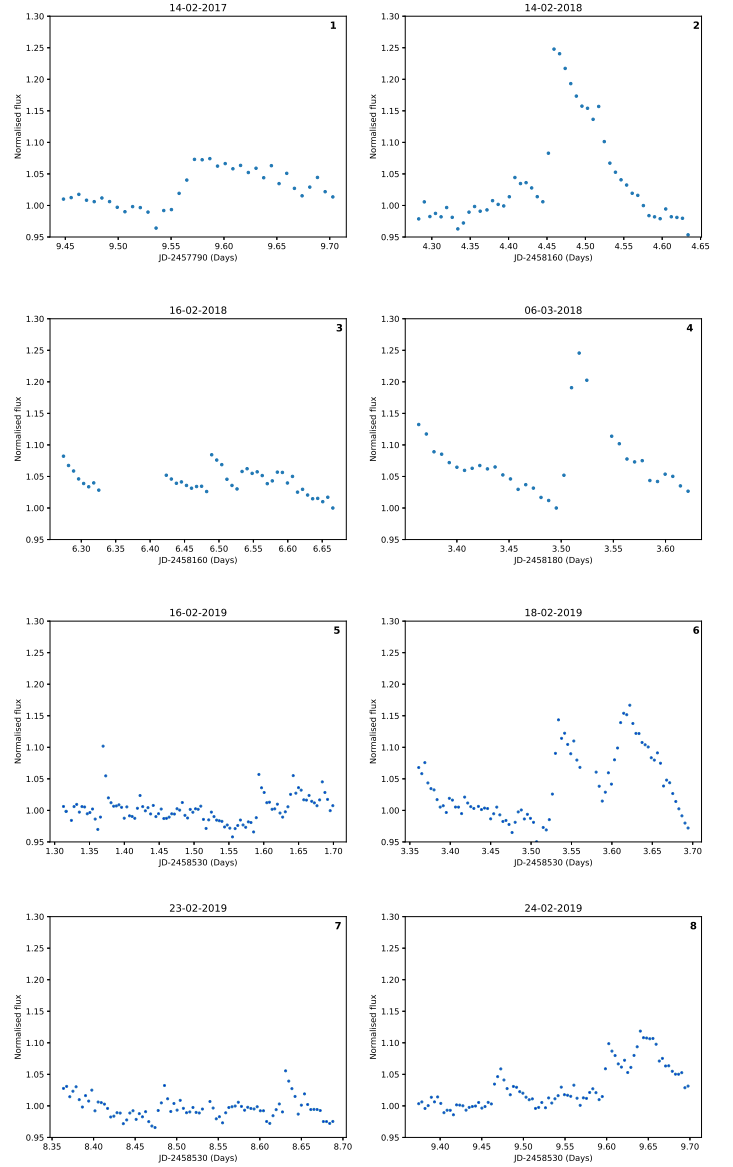


Fig. 2. Temporal evolution of the flux of the H_α line, showing light curves of the strongest observed flares.

We obtained an average flare rate of ≈ 0.092 flares per hour, ignoring nights with fewer than six spectra. However, as we explain in section 3.2, flares have a power-law distribution, which means that the number of flares that are detected depends on the sensitivity of the measurements. The flare rates of solar observations are much higher than those of stellar observations because the Sun is much brighter and we cannot spatially resolve the stellar disc for stellar observations. When we consider only 2018 and 2019, we obtain a slightly higher rate of ≈ 0.107 flares per hour. Generally, the activity levels are much lower than those obtained in other studies e.g., $f = 0.57$ (Pettersen et al. 1984), $f > 0.71$ (Crespo-Chacón et al. 2006) and $f \sim 0.1$ (Hunt-Walker et al. 2012), where f is the frequency of flares per hour.

Buccino et al. (2014) obtained two possible activity cycles for AD Leo: one of seven years, and another less significant cycle of two years. The seven-year cycle reached a minimum in 2007, and the authors predicted that the next minimum would be in 2015 and that the stellar activity would be even lower. This

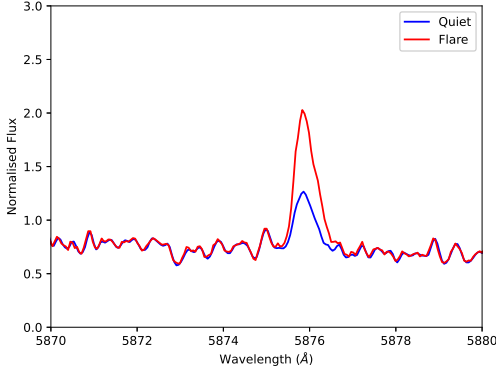


Fig. 3. Extracted spectrum of AD Leo showing the enhancement in the He I 5876 emission line during the flare in panel 2 of Fig. 2.

might explain why the activity levels were low in 2016 to 2017 and have started to increase beginning in 2018.

3.2. Flare energies

In order to estimate the energy released during a flare, we integrated the luminosity over the flare duration. The absolute line fluxes were computed from the flux of each line and its nearby continuum. The continuum flux near the emission lines was determined using direct scaling of the flux-calibrated spectrum of AD Leo from Cincunegui & Mauas (2004), assuming the same brightness of the star over time because AD Leo has very small photometric variations of ≈ 0.04 mag (Buccino et al. 2014). If the continuum were to increase during the flare, the relative strength of the line would decrease. By assuming the continuum is constant, we therefore obtain a lower limit for the line flux and thus the flares might be more energetic than estimated. To obtain the luminosities, we used the distance to the star of 4.9660 ± 0.0017 pc from *Gaia* (Gaia Collaboration et al. 2018). The estimated values of the energy released in each observed flare are also shown in Table 1. The energies given in Table 1 are for H_α , H_β , and He I 5876. The smallest flare we detected had an energy of $3.19 \pm 0.01 \times 10^{31}$ erg in H_α , $8.40 \pm 0.01 \times 10^{30}$ erg in H_β and $9.93 \pm 0.05 \times 10^{29}$ erg in He I 5876.

Fig. 4 shows the cumulative frequency distribution diagram for the observed flares. The cumulative frequency distribution of flares follows a Pareto distribution and can be fitted by a linear relation,

$$\log \nu = a + \beta \log E, \quad (1)$$

where ν is the cumulative frequency of flares with an energy E or greater and β is the power-law exponent. The more energetic flares occur less frequently, as shown by several photometric studies (e.g. Lacy et al. 1976; Pettersen et al. 1984; Hunt-Walker et al. 2012). The lines in Fig. 4 are the formal fits of a straight line (Eqn. 1) to the data to give a scale.

We obtained a value of $\beta = -0.98 \pm 0.21$ for the flares in H_α and $\beta = -0.97 \pm 0.06$ in H_β . This is close to what has previously been obtained for AD Leo, for instance, -0.82 ± 0.27 (Lacy et al. 1976), 0.85 (Audard et al. 2000), and -0.68 ± 0.16 (Hunt-Walker et al. 2012). However, our fit is steeper probably because we sample low-energy events better. Figure 4 shows that the last five points bend over. The cumulative frequency distribution bends over probably because we miss some flares close to

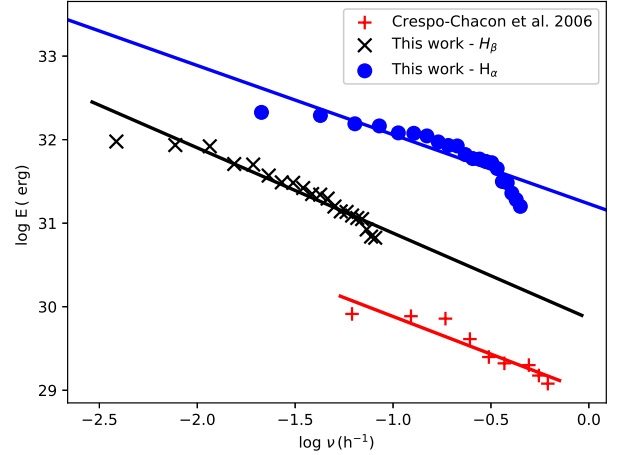


Fig. 4. Cumulative flare frequency distribution for AD Leo. The solid lines represent our best linear least-squares fit to each of the Flare Frequency Distributions. Our observations of flares in H_β (black crosses) show a similar value of β (-0.97 ± 0.06) to that of Crespo-Chacón et al. (2006) i.e., $\beta = -0.96 \pm 0.14$ (red plus symbols) who also observed in H_β .

the sensitivity limit. When we ignore these points in the fitting, the slope changes by ~ 0.58 for the flares in H_α .

In Fig. 4 we also show the flare frequency distributions for the flares in H_β for this work and that of Crespo-Chacón et al. (2006). Crespo-Chacón et al. (2006) observed AD Leo for 16.2 h in H_β , and despite the longer period of observation for this work, the two data sets show substantial agreement in the distribution of flares on AD Leo. We obtained a value of $\beta = -0.96 \pm 0.14$ for the data obtained from Crespo-Chacón et al. (2006), which is similar to the value we obtained for the flares in H_β for this work. AD Leo was on average more active during our observation time than on April 2-5, 2001 when Crespo-Chacón et al. (2006) observed it. Because the last maximum as observed by Buccino et al. (2014) was in 2011, it is expected that there also was a maximum in about 2018, which falls in our time of observations.

According to Gizis et al. (2017), the slope of the fit is greatly influenced by the energy range of the flares. A maximum likelihood estimation gives a better prediction of the value of α , especially for heavy tailed power-law distributions. The value of α is obtained from the equation

$$\alpha = 1 + n \left[\sum_{i=1}^n \ln \frac{E_i}{E_{min}} \right]^{-1}. \quad (2)$$

From $\beta = 1 - \alpha$ (Hawley et al. 2014), we obtained values of $\beta = -1.45 \pm 0.26$ for the flares in H_α , -1.12 ± 0.35 in H_β , and -1.01 ± 0.44 for data from Crespo-Chacón et al. (2006). The discrepancy in the values to those obtained from the least-squares fitting especially for H_α is probably due to the fact that it has a heavy tailed distribution. This may be attributed not only to the closeness to the sensitivity limit, but also to the fact that some values of the energy were a lower limit when only the impulsive phase was observed. When we account for the bias caused by the smallness of the samples, as in Gizis et al. (2017), we obtain new values of $\beta = -1.23 \pm 0.33$, -0.92 ± 0.26 , and -0.57 ± 0.33 , respectively. Within the error ranges, these values are rather similar to those obtained from the least-squares fitting. Table 2 gives

Table 1. Observation log showing nights of observation of AD Leo. The number of hours per night and the corresponding number of spectra obtained are shown in Cols. 3 and 5, respectively. Columns 6, 7, and 8 correspond to the estimated energies for the flares observed in H_α , H_β , and He I 5876.

Obs. date	Start–End time (UTC)	Obs (h)	Exposure time (s)	Number of Spectra	Flare Energy (10^{31} erg)		
					H_α	H_β	He I 5876
2016-11-19	01:29 - 03:47	2.33	600	14	-	-	-
2016-11-20	00:01 - 00:32	0.5	600	3	-	-	-
2016-12-09	01:17 - 01:47	0.5	600	3	-	-	-
2016-12-16	23:25 - 01:30	2	600	12	-	-	-
2016-12-21	01:23 - 04:55	3.5	600	21	-	-	-
2017-02-03	23:54 - 00:15	0.33	600	2	-	-	-
2017-02-04	22:19 - 00:03	1.83	600	11	-	-	-
2017-02-13	01:11 - 04:21	3.17	600	19	-	-	-
2017-02-14 [†]	22:37 - 04:44	6	600	36	12.05 ± 0.03	9.495 ± 0.077	0.553 ± 0.004
2017-02-15	22:58 - 04:26	5.33	600	32	-	-	-
2017-03-10	20:41 - 21:01	0.33	600	2	-	-	-
2017-03-10	18:51 - 01:51	6.83	600	41	-	-	-
2017-03-11	18:14 - 03:15	8.67	600	52	-	-	-
2017-03-12	18:25 - 02:24	3.83	600	23	-	-	-
2017-04-15	21:41 - 23:15	1.67	600	10	-	-	-
2017-05-03	20:55 - 21:25	0.5	600	3	-	-	-
2017-05-06	19:33 - 22:21	2.83	600	17	-	-	-
2017-05-07	19:17 - 20:20	1.17	600	7	-	-	-
2017-05-09	20:55 - 21:26	0.5	600	3	-	-	-
2017-05-10	20:16 - 21:19	1.17	600	7	-	-	-
2017-05-15 [†]	20:31 - 21:47	1.25	600	8	1.593 ± 0.005	-	-
2017-12-24	02:25 - 03:07	0.5	600	3	-	-	-
2017-12-25	23:53 - 05:07	3.67	600	22	-	-	-
2017-12-26	00:37 - 01:40	1.33	600	7	-	-	-
2017-12-28	22:53 - 00:06	1.25	600	8	-	-	-
2018-01-05	01:28 - 03:45	2.33	600	14	-	-	-
2018-02-12	19:25 - 23:23	2.67	600	16	-	-	-
2018-02-13 [†]	18:29 - 04:48	10	600	60	3.155 ± 0.033	1.154 ± 0.012	0.154 ± 0.002
2018-02-14	18:39 - 03:04	8.17	600	49	5.854 ± 0.031	2.195 ± 0.036	0.443 ± 0.007
					21.2 ± 0.4	8.323 ± 0.319	1.998 ± 0.077
2018-02-16 [†]	18:26 - 03:50	7	600	42	19.472 ± 0.079	5.11 ± 0.06	0.428 ± 0.002
2018-02-18	18:25 - 01:03	5.83	600	35	11.909 ± 0.082	3.715 ± 0.069	0.391 ± 0.003
2018-02-26	21:04 - 04:17	7	600	42	14.599 ± 0.061	3.081 ± 0.021	0.499 ± 0.004
2018-02-27	18:22 - 04:05	9.33	600	56	-	-	-
2018-02-28	18:19 - 04:20	9.67	600	58	-	-	-
2018-03-01	18:14 - 04:00	9.33	600	56	-	-	-
2018-03-04	00:15 - 02:21	2.17	600	13	-	-	-
2018-03-05	20:35 - 02:47	5.67	600	34	8.406 ± 0.135	5.031 ± 0.255	0.536 ± 0.013
2018-03-08	23:03 - 03:46	3.5	600	21	-	-	-
2018-03-24	18:35 - 02:16	6.92	300	83	-	-	-
2018-03-29	19:47 - 01:36	4.58	300	55	-	-	-
2018-04-23	19:34 - 23:21	3.5	300	42	-	-	-
2018-04-27 [†]	19:43 - 22:22	2.5	300	30	1.913 ± 0.022	0.691 ± 0.035	0.069 ± 0.004
2018-04-29	19:42 - 22:21	2.5	300	30	-	-	-
2018-05-01	19:58 - 22:37	2.5	300	30	-	-	-
2018-05-04	19:56 - 22:35	2.5	300	30	-	-	-
2018-05-05	19:59 - 22:11	2.08	300	25	-	-	-
2018-05-07	19:52 - 22:31	2.5	300	30	-	-	-
2019-02-13	23:28 - 04:31	4.83	300	58	-	-	-
2019-02-14	19:12 - 04:38	8.67	300	104	8.518 ± 0.025	2.234 ± 0.013	0.524 ± 0.002
2019-02-15	19:31 - 04:53	8.67	300	104	-	-	-
2019-02-16	19:22 - 04:38	8.58	300	103	4.505 ± 0.041	1.12 ± 0.01	0.123 ± 0.001
					3.19 ± 0.01	0.84 ± 0.01	0.099 ± 0.0005
					3.860 ± 0.023	8.61 ± 0.01	0.126 ± 0.001
					5.531 ± 0.019	1.364 ± 0.012	0.192 ± 0.0008
2019-02-17 [†]	19:23 - 04:18	8.33	300	100	6.628 ± 0.039	1.97 ± 0.02	0.300 ± 0.003
					2.884 ± 0.019	0.669 ± 0.008	0.100 ± 0.0003
2019-02-18	20:31 - 04:31	7	300	84	15.479 ± 0.012	3.045 ± 0.049	0.408 ± 0.002
2019-02-23	20:35 - 04:22	7.08	300	85	5.939 ± 0.017	1.385 ± 0.008	0.466 ± 0.002
					5.295 ± 0.032	1.235 ± 0.018	0.419 ± 0.005
2019-02-24 [†]	20:5 04:36	7.17	300	86	5.488 ± 0.023	1.582 ± 0.013	0.145 ± 0.0009
					11.083 ± 0.048	2.636 ± 0.043	0.292 ± 0.002
2019-02-25	20:39 - 02:12	5.08	300	61	-	-	-

[†] indicates nights in which the value of the energy is a lower limit as only the impulsive phase or part of the gradual phase was observed.

Table 2. Summary of the β values obtained using the different techniques. l.s.f is least-squares fitting, and m.l.e is maximum likelihood estimation. ^a implies least-squares fitting considering all data points, ^b is least-squares fitting ignoring 5 points with lowest energy, ^c implies maximum likelihood estimation with bias and ^d is maximum likelihood estimate without bias. H_β^+ corresponds to data from Crespo-Chacón et al. (2006)

Method	β value		
	H_α	H_β	H_β^+
l.s.f ^a	-0.98 ± 0.21	-0.97 ± 0.06	-0.96 ± 0.14
l.s.f ^b	-1.56 ± 0.13	-1.10 ± 0.08	–
m.l.e ^c	-1.45 ± 0.26	-1.12 ± 0.35	-1.01 ± 0.44
m.l.e ^d	-1.23 ± 0.33	-0.92 ± 0.26	-0.57 ± 0.33

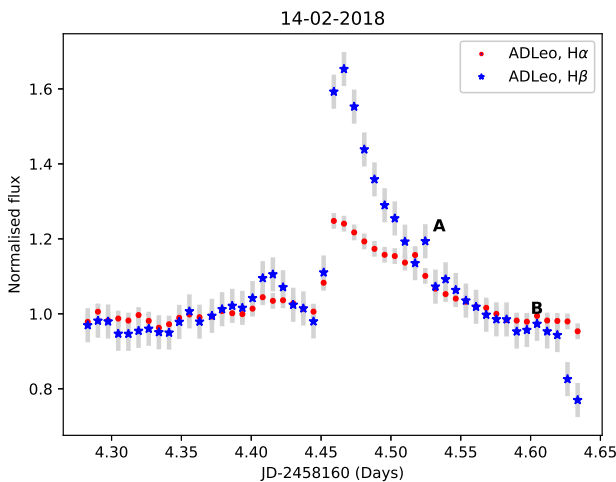


Fig. 5. Light curves of the flare observed on February 14, 2018, in H_α (filled red circles) and H_β (filled blue stars).

a summary of the β values obtained using the different techniques.

The ratio of the energy in H_α to the energy in H_β does not depend on the energy of the events. We obtained an average flux ratio of 3.36 ± 0.26 . With this ratio, we are able to correlate the energy in the Balmer lines to that in the X-ray also using the ratio of the energy in H_β to that in H_γ (1.82 ± 0.18 , Crespo-Chacón et al. 2006). The luminosity in X-ray can be related to the luminosity in H_γ from the relation $L_x(0.04 \text{ to } 2.0 \text{ keV}) = 31.6 L_{H_\gamma}$ (Butler 1993). We also calculated the average flux ratios of the He I 5876/ H_α as 0.0445 ± 0.022 and He I 5876/ H_β as 0.145 ± 0.085 . There is no correlation observed between the total line flux and these ratios. The largest flare was observed in the night of February 14, 2018. In that night, we monitored AD Leo continuously from 18:39 UT to 03:14 UT. During that time, we obtained 49 spectra with an exposure time of 600 s.

The total emission during the flare was 2.9×10^{31} erg in H_β and 2.12×10^{32} erg in H_α . As we discuss below, flares of this size certainly affect planetary atmospheres. During the decay phase of the flare, two events that we may classify as weak events were observed. The first, marked as A in Fig. 5, lasted about 7.2×10^3 s, and event B lasted about 3×10^3 s. These weak post-flare events tend to occur during large CMEs on the Sun as a result of the movement of magnetic loop footpoints that form current sheets and in this way trigger other smaller events (Kovári et al.

2007). Pre-flare dips are also observed before the impulsive phase of almost all the flares that were observed, including this large flare. The dips last for about 10–30 min. The duration of these dips is consistent with those presented in literature (e.g. Ventura et al. 1995; Leitzinger et al. 2014). These dips might be a result of variations in the H_α flux due to pre-flare stellar activity (Leitzinger et al. 2014). CMEs on the Sun are commonly associated with very energetic flares (Yashiro & Gopalswamy 2009).

3.3. Line asymmetries

In order to detect CMEs, we searched for line asymmetries by visual inspection of the average subtracted spectra. We also measured the position of the line centre at each intensity, thus obtaining accurate radial velocities at each intensity level. We observed line asymmetries (in red and in blue) and broadening of wings in several spectra during flares. Table 3 gives a summary of the asymmetries observed and the velocities determined.

We found 75 spectra with line asymmetries. Three large events were found, and these corresponded to nights with large flare events. However, there were nights with weak or no flares, but the spectra showed some asymmetry. This asymmetry could be interpreted as multiple chromospheric condensations that may result from unresolved low-energy flares (Crespo-Chacón et al. 2006). To determine the velocities of the events, we subtracted the spectra for each night from the spectrum in quiescence (an average of the spectra without enhancement in H_α) and calculated the Doppler shift in the red and blue of the H_α emission line. The maximum velocity is determined at the point where the continuum of the residual spectrum merges with the continuum of the spectrum in quiescence. In searching for CMEs, we looked for asymmetries in the blue wings of emission lines because they are often used as a possible signature. The escape velocity of AD Leo is $\approx 590 \pm 11 \text{ km s}^{-1}$, and a sign of a CME would be a blue-shifted component with a velocity greater than this value. Fig. 6 shows the evolution of the different emission line profiles during the strongest flare after subtracting the spectra in quiescence. There is an increase in the flux at the impulsive phase, however, the core of the lines increases faster than the wings. The emission lines also broaden during the impulsive phase of the flare and decrease with flare evolution. The broadening of the lines might be a result of the Stark broadening effect (Švestka 1972; Gizis et al. 2013) and turbulent motions in the chromosphere of the star (Kowalski et al. 2017). In the impulsive phase, the blue wing is more strongly enhanced, but as the flare decays, more enhancement is observed in the red wing. We also note that the continuum does not change much in quiescence and during the flares. These flares, known as non-white flares, are common on the Sun and have previously been observed on AD Leo (e.g. Crespo-Chacón et al. 2006). However, we may not completely rule out the fact that the continuum changed because there was no simultaneous photometry. In Fig. 7 we show the temporal evolution of the bulk velocity (using a bisector) of the helium line during the largest flare. This line is an indicator of a very hot plasma, and the asymmetry was more pronounced in this line than in the H_α and H_β lines. The bulk velocities of the plasma in the impulsive phase ranged between $8 - 10 \text{ km s}^{-1}$.

Table 3. Summary of the line asymmetries in H α with the determined velocities in km s⁻¹. The number of the spectra column corresponds to the number of spectra per night in which asymmetries were observed. The average velocities in the blue and red were obtained from the corresponding spectra.

Date	Velocity-Blue (km s ⁻¹)			Velocity-Red (km s ⁻¹)			Number of spectra	
	min	max	average	min	max	average	blue	red
2017-05-15	156	176	170	157	163	161	7	7
2018-02-13	–	–	176	–	–	–	1	–
2018-02-14	62	269	128	100	194	154	10	14
2018-03-02	103	–	–	135	138	137	1	4
2018-03-06	118	194	160	141	326	219	3	4
2019-02-14	99	122	107	–	–	–	5	–
2019-02-15	93	108	101	105	121	113	3	3
2019-02-16	101	201	138	192	194	193	6	2
2019-02-17	89	143	106	114	135	127	6	3
2019-02-18	89	201	140	102	196	150	18	12
2019-02-23	103	140	127	–	–	–	3	–
2019-02-24	83	131	91	114	150	132	4	2

4. Discussion

4.1. Line asymmetries

In general, asymmetries can be interpreted as a signature of chromospheric plasma motions. Blue asymmetry is usually interpreted as upward-moving material, whereas a red asymmetry can be associated with downward motions (chromospheric condensation) (Canfield et al. 1990; Heinzel et al. 1994; Crespo-Chacón et al. 2006; Kuridze et al. 2016; Fuhrmeister et al. 2018). During the impulsive phase, the broad component appears blue-shifted up to ~ 260 km s⁻¹ and is then red-shifted up to ~ 190 km s⁻¹ during the gradual decay phase (see Fig. 6). These asymmetries have been observed in this and other M stars by several authors (e.g. Houdebine et al. 1990, 1993; Gunn et al. 1994; Guenther & Emerson 1997; Montes et al. 1999; Fuhrmeister & Schmitt 2004; Fuhrmeister et al. 2005; Crespo-Chacón et al. 2006; Leitzinger et al. 2014; Vida et al. 2016; Fuhrmeister et al. 2018). We found that the observed velocities of the blue asymmetry events were between $80 - 260$ km s⁻¹, which is far below the escape velocity of the star. This implies that none of these are CME events. The slow events can be attributed to three origins that we describe below.

- (i) Chromospheric evaporation may be one origin, as discussed by Fuhrmeister et al. (2018). During flare onset, material rises with a different velocity, producing the broad component of the line, and as the flare decays, the material flows downwards, leading to the red asymmetry that is observed (Fuhrmeister et al. 2008). The authors interpreted this scenario as a chromospheric prominence that is lifted during flare onset and then rains down during decay. During solar flares, the velocities of chromospheric evaporation reach several tens of km s⁻¹ and in extremes, even to a few hundred km s⁻¹.
- (ii) The velocities we obtained are projected velocities because the propagation angle of the CMEs is unknown (Leitzinger et al. 2010).
- (iii) Magnetic field confinement of CMEs in very active stars is another cause (Drake et al. 2016; Alvarado-Gómez et al. 2018). Alvarado-Gómez et al. (2018) suggested that the strong magnetic fields on active stars do not allow material to leave the stellar surface. Only monster CMEs with energies greater than 3×10^{32} erg may escape a strong field of 75 G. Previous studies showed that AD Leo has a magnetic field of

strength $B \sim 3300$ G (Cranmer & Saar 2011, and references therein) and an average magnetic field of $\sim 300 - 330$ G (Lavail et al. 2018), which is stronger than the field (75 G) used in the model of Alvarado-Gómez et al. (2018). This implies that CMEs on AD Leo require vast energy to escape this magnetic field. The authors further stated that eruptions following the solar flare–CME relation can only occur during flare events with energies higher than 6×10^{32} erg (e.g. Guenther & Emerson 1997), but the energy in the largest event we observed was one-third of this in H α . The overlying field in active stars reduces the CME speeds in comparison with the solar observations and their extrapolations. In addition to this, Chen et al. (2006) found in their CME velocity distribution study on the Sun that CMEs that were associated with non-active region filaments had higher eruption speeds than those with active region filaments. This shows that the magnetic field configuration plays an important role in CME propagation.

Red asymmetries usually occur at the impulsive phase of flares on the Sun and are driven by non-thermal downward electron beams (e.g. Ichimoto & Kurokawa 1984; Canfield et al. 1990; Heinzel et al. 1994). These red-shifted downflows in the cool lines on the Sun with velocities in the order of ~ 100 km s⁻¹ have been interpreted as solar chromospheric condensations. This condensation is often associated with explosive evaporation. During explosive evaporation, the chromosphere is unable to radiate the flare energy away, and this results in excess pressure that causes plasma to move downwards (Milligan et al. 2006).

On the other hand, these asymmetries may not solely be attributed to chromospheric flows, but also to opacity changes occurring at different wavelengths because the velocity gradients in the chromosphere are very steep. This leads to the formation of blue and red asymmetries (Kuridze et al. 2015).

The low bulk velocities obtained from the bisector of the largest event might also be an indication that material may not be rising or falling. Rather, there is a movement in the flare footpoints that causes the red and blue asymmetries. During flare reconnection, the flare footpoints mostly appear to move away from one another (Asai et al. 2004; Temmer et al. 2007). To understand this better, we need photometric observations. Thus, there is need for simultaneous photometry and spectroscopy to fully understand the processes taking place in the photosphere and the chromosphere on this star during flare events.

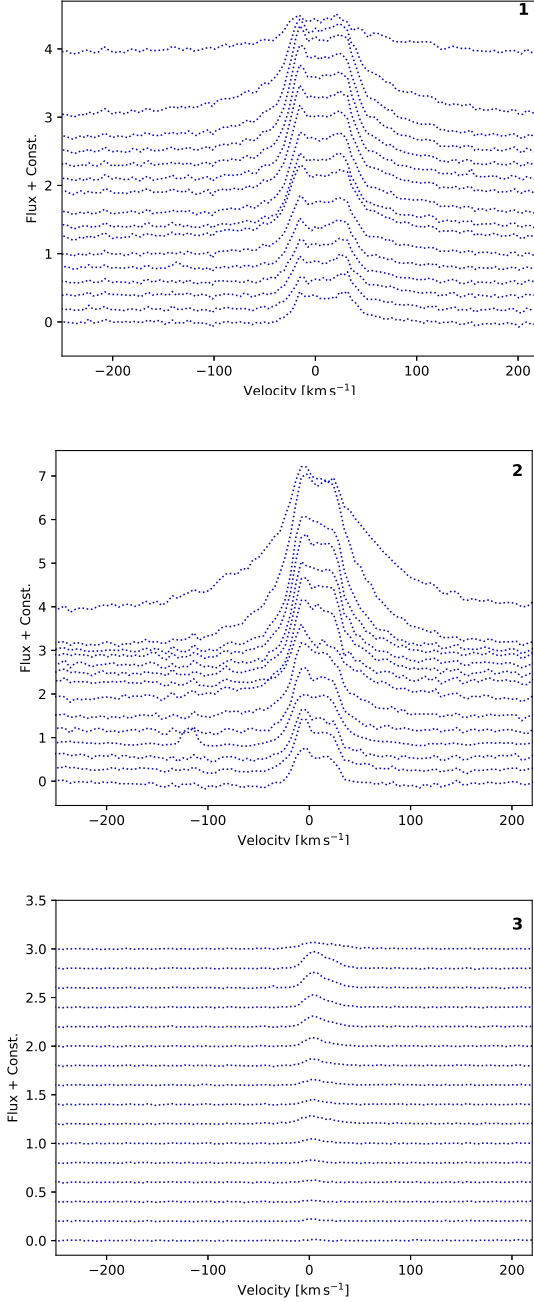


Fig. 6. Evolution of the chromospheric lines: H_α (panel 1), H_β (panel 2), and He I 5876 (panel 3) during the strongest flare.

Vida et al. (2019) studied 21 high-resolution spectra of AD Leo in their search for CMEs in late-type stars. In the 21 spectra, they found 9 events with low velocities with a maximum of 195 km s^{-1} in the blue and 296 km s^{-1} in the red, which is far below the escape velocity of AD Leo. Although their sample is smaller, their findings are in agreement with our findings. This might imply that fast events are rare on this and other M stars, and solar flare–CME relations may therefore not be extended to M stars.

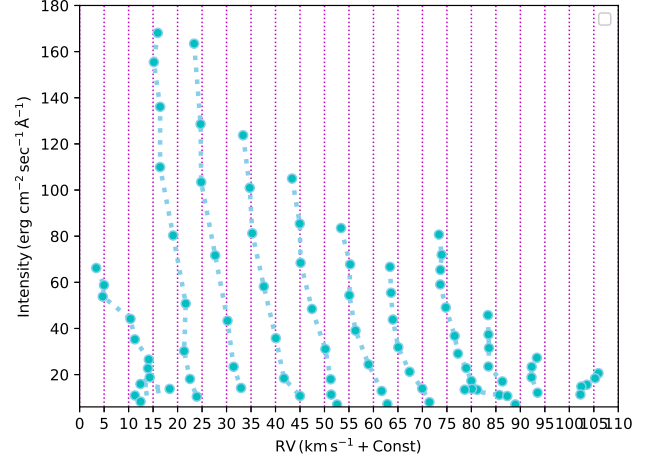


Fig. 7. Evolution of the bisector of the He I line during the strongest flare.

4.2. Flares and their effect on habitability

Coronal mass ejections are commonly associated with flares that release energy in 10^{32} erg and last $\approx 10^4$ s. The total emission during the largest flare that we observed was 2.9×10^{31} erg in H_β and 2.12×10^{32} erg in H_α . In the case of solar flares, the energy released in soft X-rays and UV is one order of magnitude higher than that in H_α (see reviews by Mirzorian 1984; Haisch 1999; Garcia Alvarez 2000; Benz & Güdel 2010). Because the largest flare had 2.12×10^{32} erg in H_α , the flux in the X-ray and UV is expected to be $\approx 2.12 \times 10^{33}$ erg. According to Somov (1992), the largest solar flares have 3×10^{30} erg in H_α , which means that this flare was 70 times more energetic. From the flare frequency distribution we obtained for flares on this star, about one event with an energy of 3×10^{30} erg occurs per hour. On the Sun, many X class flares occur during solar maximum, but only a few or none during minimum. The average number of X class flares per year given in Aschwanden & Freeland (2012) is ≈ 6.7 , which translates into 0.000765 events per hour. This implies that the flare activity of AD Leo is 1 000 times higher than that of the Sun for very large flares.

Using the parallax of AD Leo from *Gaia*, we obtain a distance of 4.9660 ± 0.0017 pc, radius of $0.444 R_\odot$, and luminosity of $0.024 L_\odot$. Following the method of determining the habitable zone boundaries in Whitmire & Reynolds (1996), we estimated its habitable zone to be at about 0.2 AU. Considering the largest flare, its intensity would be 2 000 times higher for a planet in the habitable zone. This means that an Earth-size planet in the habitable zone of AD Leo would receive more than 10^6 times as much energy than the Earth does from solar flares. The total energy of the observed flares is $\approx 1.77 \times 10^{33}$ erg during our observation time. In a year, the star would emit 35 times as much energy, which means the star would emit $\approx 6.2 \times 10^{34}$ erg. When we consider a planet with the radius of the Earth in the habitable zone, the planet would receive at least $\approx 2.6 \times 10^{28}$ erg per year in soft X-rays and XUV radiation.

Segura et al. (2010) analysed the effect of one flare with a total energy of $\sim 10^{34}$ erg that was observed on AD Leo in 1985. They found that the event did not necessarily present a problem for life on the surface of an Earth-like planet through the UV radiation. However, a substantial decrement in the ozone ($\sim 94\%$) was noted, caused by protons that would be produced if there

were a CME. The authors estimated that the recovery time for the effects of such a flare is about 50 years. Venot et al. (2016) studied the effect of the same flare on the chemical composition of two hypothetical sub-Neptune and super-Earth-like planets orbiting AD Leo. They found that a single flare event could irreversibly alter the chemical composition of warm or hot planetary atmospheres, with the final steady-state being significantly different from the initial steady-state in both cases. Tilley et al. (2017) modelled the effects of frequent flaring of an M dwarf on the atmosphere of an unmagnetised Earth-like planet in the habitable zone. They found that the impact of one flare (equivalent to the size of flares on AD Leo) per month is sufficient to drive a loss of 99.99% of the ozone column within eight years, with an unlikely recovery and thus further destruction. The surface of the planet would experience a UV flux of $\sim 0.18 - 1 \text{ W m}^{-2}$. The authors suggested further experiments to establish the impact of these fluxes on the onset of complex organic chemistry and life. Howard et al. (2018) discussed the impact of flares on the habitability of planets around Proxima Centauri. They simulated flares with energies in the range of $10^{29.5} - 10^{32.9}$ erg in the U band. They found that such events deplete the ozone by 90% and the system hardly reaches a steady state with increasing time. This may seriously question the possibility of the existence of complex life forms around these active stars because the planetary systems seem to experience a high loss of ozone during high-energy events, which leaves the planetary surfaces largely unprotected from UV light. Only organisms capable of tolerating extreme conditions can survive such an activity.

5. Summary and conclusions

AD Leo was monitored during the period from November 2016 to February 2019 whenever it was visible for one week per month, and 2002 spectra were obtained and analysed. This is the largest survey of this kind on AD Leo. We expected to observe quite a number of flares and possibly CMEs because Crespo-Chacón et al. (2006) obtained a flare frequency of AD Leo greater than 0.71 flares per hour. However, we observed that the flare rates in 2016 and 2017 were generally low and only increased beginning in February 2018. We found 22 flares with energies of $(1.59 - 21.2) \times 10^{31}$ erg in H_α and $(0.669 - 9.495) \times 10^{31}$ erg in H_β . The smallest flare had an energy of $3.19 \pm 0.01 \times 10^{31}$ erg in H_α . We also obtained a flare frequency of 0.092 flares per hour, which is lower than that obtained in previous studies. The low frequency might be attributed to a minimum in the stellar activity cycle as predicted by Buccino et al. (2014). On the other hand, the derived flare frequency distribution is consistent with other previous studies, although with a steeper power-law index that is probably due to a better sampling of low-energy events.

We further analysed the spectra by studying the behaviour of the chromospheric lines H_α , H_β , and He I 5876 in order to search for CMEs. In this, we searched for asymmetries in the lines, which might be indicators of CMEs. We found 75 spectra with asymmetries. All these asymmetries show very low velocities in the range $60 - 270 \text{ km s}^{-1}$, which is lower than the escape velocity of the star. These slow events and the occurrence frequency of the red asymmetry after the blue asymmetry may suggest that CMEs are rare on this star. It is therefore not appropriate to use the solar flare-CME relation to predict the occurrence of CMEs on this star. The strong overlying magnetic field on these stars seems to play an important role in suppressing their CME activity.

If CMEs are rare on stars in exoplanetary systems, they would not pose a great threat, especially regarding losses of planetary atmospheres. However, effects on exoplanetary atmospheres caused by flares might still be enormous because high-energy events occur frequently, especially at the maximum of the stellar activity cycles. The habitable zones lie close in, however. These effects are the subject of future study.

Acknowledgements. The authors acknowledge the International Science Program at Uppsala University for the financial support. The authors are also grateful to the Thüringer Landessternwarte Observatory, Germany for their hospitality and giving them observation time. The authors are also grateful to the anonymous referee who gave very insightful comments that have improved the quality of this work.

This work was generously supported by the Thüringer Ministerium für Wirtschaft, Wissenschaft und Digitale Gesellschaft. This research made use of the SIMBAD database, operated at CDS, Strasbourg, France. This research also made use of data from the European Space Agency (ESA) mission *Gaia* (<https://www.cosmos.esa.int/gaia>), processed by the *Gaia* Data Processing and Analysis Consortium (DPAC) (<https://www.cosmos.esa.int/web/gaia/dpac/consortium>).

References

- Aarnio, A. N., Matt, S. P., & Stassun, K. G. 2012, *The Astrophysical Journal*, 760, 9
- Alvarado-Gómez, J. D., Drake, J. J., Cohen, O., Moschou, S. P., & Garraffo, C. 2018, *ApJ*, 862, 93
- Asai, A., Yokoyama, T., Shimojo, M., & Shibata, K. 2004, *ApJ*, 605, L77
- Aschwanden, M. J. & Freeland, S. L. 2012, *ApJ*, 754, 112
- Audard, M., Güdel, M., Drake, J. J., & Kashyap, V. L. 2000, *ApJ*, 541, 396
- Barnes, R. 2017, *Celestial Mechanics and Dynamical Astronomy*, 129, 509
- Benz, A. O. & Güdel, M. 2010, *ARA&A*, 48, 241
- Bolmont, E., Selsis, F., Owen, J. E., et al. 2017, *MNRAS*, 464, 3728
- Bonomo, A. S., Zeng, L., Damasso, M., et al. 2019, *Nature Astronomy*, 3, 416
- Buccino, A. P., Petrucci, R., Jofré, E., & Mauas, P. J. D. 2014, *ApJ*, 781, L9
- Butler, C. J. 1993, *A&A*, 272, 507
- Canfield, R. C., Penn, M. J., Wulser, J.-P., & Kiplinger, A. L. 1990, *ApJ*, 363, 318
- Chen, A. Q., Chen, P. F., & Fang, C. 2006, *A&A*, 456, 1153
- Cincunegui, C. & Mauas, P. J. D. 2004, *A&A*, 414, 699
- Cohen, O., Yadav, R., Garraffo, C., et al. 2017, *ApJ*, 834, 14
- Cranmer, S. R. & Saar, S. H. 2011, *ApJ*, 741, 54
- Crespo-Chacón, I., Montes, D., García-Alvarez, D., et al. 2006, *A&A*, 452, 987
- Crosley, M. K. & Osten, R. A. 2018, *ApJ*, 856, 39
- Cully, S. L., Fisher, G. H., Abbott, M. J., & Siegmund, O. H. W. 1994, *ApJ*, 435, 449
- Drake, J. J., Cohen, O., Garraffo, C., & Kashyap, V. 2016, in *IAU Symposium*, Vol. 320, *Solar and Stellar Flares and their Effects on Planets*, ed. A. G. Kosovichev, S. L. Hawley, & P. Heinzel, 196–201
- Drake, J. J., Cohen, O., Yashiro, S., & Gopalswamy, N. 2013, *ApJ*, 764, 170
- Erkaev, N. V., Lammer, H., Odert, P., et al. 2016, *MNRAS*, 460, 1300
- France, K., S. Froning, C., L. Linsky, J., et al. 2012, *The Astrophysical Journal*, 763
- Fuhrmeister, B., Czesla, S., Schmitt, J. H. M. M., et al. 2018, *A&A*, 615, A14
- Fuhrmeister, B., Liefke, C., Schmitt, J. H. M. M., & Reiners, A. 2008, *A&A*, 487, 293
- Fuhrmeister, B. & Schmitt, J. H. M. M. 2004, *A&A*, 420, 1079
- Fuhrmeister, B., Schmitt, J. H. M. M., & Hauschildt, P. H. 2005, *A&A*, 436, 677
- Gaia Collaboration, Brown, A. G. A., Vallenari, A., et al. 2018, *A&A*, 616, A1
- García Alvarez, D. 2000, *Irish Astronomical Journal*, 27, 117
- Giampapa, M. S., Linsky, J. L., Schneeberger, T. J., & Worden, S. P. 1978, *ApJ*, 226, 144
- Gillon, M., Jehin, E., Lederer, S. M., et al. 2016, *Nature*, 533, 221
- Gizis, J. E., Burgasser, A. J., Berger, E., et al. 2013, *ApJ*, 779, 172
- Gizis, J. E., Paudel, R. R., Mullan, D., et al. 2017, *ApJ*, 845, 33
- Guenther, E. W., Barragán, O., Dai, F., et al. 2017, *A&A*, 608, A93
- Guenther, E. W. & Emerson, J. P. 1997, *A&A*, 321, 803
- Gunn, A. G., Doyle, J. G., Mathioudakis, M., Houdebine, E. R., & Avgoloupis, S. 1994, *A&A*, 285, 489
- Haisch, B. M. 1999, in *The many faces of the sun: a summary of the results from NASA's Solar Maximum Mission*, ed. K. T. Strong, J. L. R. Saba, B. M. Haisch, & J. T. Schmelz, 481
- Hatzes, A. P. & Rauer, H. 2015, *ApJ*, 810, L25
- Hawley, S. L., Allred, J. C., Johns-Krull, C. M., et al. 2003, *ApJ*, 597, 535
- Hawley, S. L., Davenport, J. R. A., Kowalski, A. F., et al. 2014, *ApJ*, 797, 121

- Hawley, S. L. & Pettersen, B. R. 1991, *ApJ*, 378, 725
- Heinzel, P., Karlicky, M., Kotrc, P., & Svestka, Z. 1994, *Sol. Phys.*, 152, 393
- Houdebine, E. R., Foing, B. H., Doyle, J. G., & Rodono, M. 1993, *A&A*, 274, 245
- Houdebine, E. R., Foing, B. H., & Rodono, M. 1990, *A&A*, 238, 249
- Howard, W. S., Tilley, M. A., Corbett, H., et al. 2018, *ApJ*, 860, L30
- Hunt-Walker, N. M., Hilton, E. J., Kowalski, A. F., Hawley, S. L., & Matthews, J. M. 2012, *PASP*, 124, 545
- Ichimoto, K. & Kurokawa, H. 1984, *Sol. Phys.*, 93, 105
- Kay, C., Opher, M., & Kornbleuth, M. 2016, *ApJ*, 826, 195
- Keenan, P. C. & McNeil, R. C. 1989, *ApJS*, 71, 245
- Kielkopf, J. F., Hart, R., Carter, B. D., & Marsden, S. C. 2019, *MNRAS*, 486, L31
- Kislyakova, K. G., Lammer, H., Holmström, M., et al. 2013, *Astrobiology*, 13, 1030
- Kovári, Z., Vilardell, F., Ribas, I., et al. 2007, *Astronomische Nachrichten*, 328, 904
- Kowalski, A. F., Allred, J. C., Uitenbroek, H., et al. 2017, *ApJ*, 837, 125
- Kuridze, D., Mathioudakis, M., Christian, D. J., et al. 2016, *ApJ*, 832, 147
- Kuridze, D., Mathioudakis, M., Simões, P. J. A., et al. 2015, *ApJ*, 813, 125
- Lacy, C. H., Moffett, T. J., & Evans, D. S. 1976, *ApJS*, 30, 85
- Lammer, H., Bredehöft, J. H., Coustenis, A., et al. 2009a, *A&A Rev.*, 17, 181
- Lammer, H., Bredehöft, J. H., Coustenis, A., et al. 2009b, *A&A Rev.*, 17, 181
- Lammer, H., Erkaev, N. V., Odert, P., et al. 2013, *MNRAS*, 430, 1247
- Lammer, H., Kasting, J. F., Chassefière, E., et al. 2008, *Space Sci. Rev.*, 139, 399
- Lammer, H., Kislyakova, K. G., Odert, P., et al. 2011, *Origins of Life and Evolution of the Biosphere*, 41, 503
- Lammer, H., Lichtenegger, H. I. M., Kulikov, Y. N., et al. 2007, *Astrobiology*, 7, 185
- Lammer, H., Stökl, A., Erkaev, N. V., et al. 2014, *MNRAS*, 439, 3225
- Lamzin, S. A. 1989, *AZh*, 66, 1330
- Lavail, A., Kochukhov, O., & Wade, G. A. 2018, *MNRAS*, 479, 4836
- Leitzinger, M., Odert, P., Greimel, R., et al. 2014, *MNRAS*, 443, 898
- Leitzinger, M., Odert, P., Hanslmeier, A., et al. 2010, *International Journal of Astrobiology*, 9, 235
- Lissauer, J. J., Fabrycky, D. C., Ford, E. B., et al. 2011, *Nature*, 470, 53
- Lloyd, R. O. P., France, K., Youngblood, A., et al. 2018, *ApJ*, 867, 71
- Lurie, J. C., Henry, T. J., Jao, W.-C., et al. 2014, *AJ*, 148, 91
- Masuda, K. 2014, *ApJ*, 783, 53
- Milligan, R. O., Gallagher, P. T., Mathioudakis, M., & Keenan, F. P. 2006, *ApJ*, 642, L169
- Mirzolian, L. V. 1984, *Vistas in Astronomy*, 27, 77
- Montes, D., Saar, S. H., Collier Cameron, A., & Unruh, Y. C. 1999, *MNRAS*, 305, 45
- Morin, J., Donati, J. F., Petit, P., et al. 2008, *MNRAS*, 390, 567
- Morin, J., Donati, J. F., Petit, P., et al. 2010, *MNRAS*, 407, 2269
- Odert, P., Leitzinger, M., Hanslmeier, A., & Lammer, H. 2017, *MNRAS*, 472, 876
- Osten, R. A. & Wolk, S. J. 2015, *ApJ*, 809, 79
- Pettersen, B. R., Coleman, L. A., & Evans, D. S. 1984, *ApJS*, 54, 375
- Roettenbacher, R. M. & Kane, S. R. 2017, *ApJ*, 851, 77
- Santerne, A., Brügger, B., Armstrong, D. J., et al. 2018, *Nature Astronomy*, 2, 393
- Segura, A., Walkowicz, L. M., Meadows, V., Kasting, J., & Hawley, S. 2010, *Astrobiology*, 10, 751
- Somov, B. V., ed. 1992, *Astrophysics and Space Science Library*, Vol. 172, Physical processes in solar flares.
- Temmer, M., Veronig, A. M., Vršnak, B., & Miklenic, C. 2007, *ApJ*, 654, 665
- Tian, F. & Ida, S. 2015, in *Pathways Towards Habitable Planets*, 20
- Tilley, M. A., Segura, A., Meadows, V. S., Hawley, S., & Davenport, J. 2017, *ArXiv e-prints*
- Tuomi, M., Jones, H. R. A., Butler, R. P., et al. 2019, *arXiv e-prints*, arXiv:1906.04644
- Venot, O., Rocchetto, M., Carl, S., Roshni Hashim, A., & Decin, L. 2016, *ApJ*, 830, 77
- Ventura, R., Peres, G., Pagano, I., & Rodono, M. 1995, *A&A*, 303, 509
- Vida, K., Kővári, Z., Pál, A., Oláh, K., & Kriskovics, L. 2017, *ApJ*, 841, 124
- Vida, K., Kriskovics, L., Oláh, K., et al. 2016, *A&A*, 590, A11
- Vida, K., Leitzinger, M., Kriskovics, L., et al. 2019, *A&A*, 623, A49
- Švestka, Z. 1972, *Sol. Phys.*, 24, 154
- Whitmire, D. P. & Reynolds, R. T. 1996, in *Circumstellar Habitable Zones*, ed. L. R. Doyle, 117
- Yashiro, S. & Gopalswamy, N. 2009, in *IAU Symposium*, Vol. 257, *Universal Heliophysical Processes*, ed. N. Gopalswamy & D. F. Webb, 233–243